

The absolute frequency of the ^{87}Sr optical clock transition

Gretchen K. Campbell, Andrew D. Ludlow, Sebastian Blatt, Jan W. Thomsen, Michael

J. Martin, Marcio H. G. de Miranda, Tanya Zelevinsky, Martin M. Boyd, Jun Ye

JILA, National Institute of Standards and Technology and University of Colorado,

Department of Physics, University of Colorado, Boulder, Colorado 80309-0440, USA

Scott A. Diddams, Thomas P. Heavner, Thomas E. Parker, Steven R. Jefferts

National Institute of Standards and Technology,

Time and Frequency Division, 325 Broadway, Boulder, Co 80305, USA

(Dated: October 26, 2018)

The absolute frequency of the $^1S_0-^3P_0$ clock transition of ^{87}Sr has been measured to be 429 228 004 229 873.65 (37) Hz using lattice-confined atoms, where the fractional uncertainty of 8.6×10^{-16} represents one of the most accurate measurements of an atomic transition frequency to date. After a detailed study of systematic effects, which reduced the total systematic uncertainty of the Sr lattice clock to 1.5×10^{-16} , the clock frequency is measured against a hydrogen maser which is simultaneously calibrated to the US primary frequency standard, the NIST Cs fountain clock, NIST-F1. The comparison is made possible using a femtosecond laser based optical frequency comb to phase coherently connect the optical and microwave spectral regions and by a 3.5 km fiber transfer scheme to compare the remotely located clock signals.

I. INTRODUCTION

In recent years optical atomic clocks have made great strides, with dramatic improvements demonstrated in both stability and accuracy, and have now surpassed the performance of the best microwave standards [1, 2]. Optical clock candidates are being investigated by a variety of groups using a number of different atomic transitions in trapped ions [2, 3, 4, 5, 6], trapped neutral atoms, and freely expanding neutral atoms [1, 7, 8, 9, 10, 11, 12, 13]. As the best optical standards now support an accuracy surpassing that of the Cs primary standards (3.3×10^{-16}) [14, 15, 16], it becomes imperative to directly compare these optical standards against each other [1, 2] to evaluate them at the lowest possible level of uncertainties. Nevertheless, it still remains important

that these optical standards are evaluated by the mature primary Cs standards for multiple reasons.

First, the accuracy of frequency standards is ultimately defined by the Cs clock under the current realization of the SI-second. Additionally, over the years a remarkable infrastructure has been developed to support the transfer of Cs standards for international intercomparisons, and the primary frequency standards at multiple national labs all agree within their stated uncertainties [17]. While fiber networks [18, 19, 20, 21] now provide the most precise frequency distribution links between optical clocks located near each other (for example within 100 km), for intercontinental comparisons optical clocks need to be measured relative to Cs standards. In fact, recent intercomparisons of Sr clocks among three laboratories at JILA, SYRTE, and University of Tokyo [22] have reached an agreement at 1×10^{-15} , approaching the Cs limit. This has firmly established the Sr lattice clock standard as the best agreed-upon optical clock frequency to date, and second only to the Cs standard itself among all atomic clocks.

Second, an important application of highly accurate atomic clocks is the test of fundamental laws of nature with high precision. For example, atomic clocks are placing increasingly tighter constraints on possible time-dependent variations of fundamental constants such as the fine-structure constant (α) and the electron-proton mass ratio (μ) [2, 22, 23, 24, 25, 26, 27, 28, 29]. These measurements are made by comparing atomic transition frequencies among a diverse set of atomic species, helping reduce systematic effects. For example, an optical clock transition frequency is generally sensitive to variations of α , with different atoms having different sensitivities [30]. Sr in fact has a rather low sensitivity. The Cs standard on the other hand is based on a hyperfine transition and is sensitive to variations in both α and μ . Thus measurement of the frequency ratio of Sr and Cs over the course of a year limits not only the possible linear drift of these constants but also constrains possible coupling between fundamental constants and the gravitational potential, which would signal a violation of local position invariance [22, 29, 31, 32].

In recent years, the most accurate absolute frequency measurements were performed using single trapped ions. These systems benefit from the insensitivity of the ions to external perturbations, and using Hg^+ ions a frequency uncertainty of 9.1×10^{-16} [3] has been achieved. Large ensembles of neutral atoms offer high measurement signal to noise ratios, however, neutral atom systems have typically been limited by motional effects. By confining the atoms in an optical lattice [7, 8, 9] these effects are greatly reduced, as the atoms can be trapped in the Lamb-Dicke regime, where both Doppler and photon-recoil related effects are suppressed. One such system is the ^{87}Sr $(5s^2)^1S_0 - (5s5p)^3P_0$ transition, which is currently being pursued by a number of groups

worldwide [1, 33, 34, 35].

In this paper we report on the absolute frequency measurement of the $^{87}\text{Sr } ^1S_0-^3P_0$ clock transition. The absolute frequency is measured using a femtosecond laser based octave-spanning optical frequency comb to compare the ^{87}Sr optical transition frequency to a hydrogen maser, which is simultaneously calibrated to the NIST fountain primary frequency standard, NIST-F1. To remotely link the Sr standard, which is located at JILA on the University of Colorado campus, to the NIST-F1 Cs clock, located at the NIST Boulder laboratories, a 3.5 km optical fiber link is used to transfer the H-maser reference signal [36, 37]. In addition to demonstrating one of the most accurate measurements of an optical transition frequency to date, the agreement of this result with previous measurements both at JILA and around the world demonstrates the robustness and reproducibility of strontium as a frequency standard, and as a future candidate for the possible redefinition of the SI second.

II. EXPERIMENTAL SETUP

The frequency standard uses lattice-confined ^{87}Sr atoms with nuclear spin $I = 9/2$. Although the ^{87}Sr apparatus has been previously described elsewhere [8, 33], here we summarize the experimental details most relevant to this work. To measure the frequency of the clock transition, ^{87}Sr atoms are first trapped and cooled to mK temperatures in a magneto-optical trap (MOT) operated on the $^1S_0-^1P_1$ strong 461 nm cycling transition (see Fig. 1a for a diagram of relevant energy levels). The atoms are then transferred to a second stage 689 nm MOT for further cooling. This dual-frequency MOT uses narrow line cooling [38, 39], resulting in final temperatures of $\sim 1 \mu\text{K}$. During the cooling process, a one-dimensional optical lattice is superimposed in the nearly vertical direction. After the second MOT stage, the MOT optical beams and the inhomogeneous magnetic field are turned off, leaving $\sim 10^4$ atoms at $2.5 \mu\text{K}$ trapped in the optical lattice. The optical lattice is created using a retro-reflected laser beam and is operated near a laser frequency where the polarizability of the 1S_0 and 3P_0 states are identical for the lattice field [40, 41]. For this work, the lattice is operated at a trap depth of $U_T = 35E_{rec}$, where $E_{rec} = \hbar^2 k^2 / 2m$ is the lattice photon recoil energy and $k = 2\pi/\lambda$ is the wavevector of the lattice light. At this lattice depth the atoms are longitudinally confined in the Lamb-Dicke regime and in the resolved sideband limit [42]. Spectroscopy is performed by aligning the probe laser precisely along the axis of the lattice standing wave, and the atoms are probed free of recoil or motional effects. The vertical orienta-

tion of the lattice breaks the energy degeneracy between lattice sites, strongly prohibiting atomic tunneling [43].

Before performing spectroscopy, the atoms are first optically pumped to the stretched $|F = 9/2, m_F = \pm 9/2\rangle$ states with the use of a weak optical beam resonant with the $^1S_0(F = 9/2) \rightarrow ^3P_1(F = 7/2)$ transition. Here $\vec{F} = \vec{I} + \vec{J}$ is the total angular momentum, with \vec{I} the nuclear spin and \vec{J} the total electron angular momentum. The beam used for optical pumping is aligned collinear with the lattice, and is linearly polarized along the lattice polarization axis. The optical pumping is performed with a small magnetic bias field ($\sim 3 \mu\text{T}$), which is also oriented along the lattice polarization. After optical pumping, spectroscopy is performed on the $^1S_0 \rightarrow ^3P_0$ clock transition from the two spin sublevels. The clock transition, which has a theoretical natural linewidth of $\sim 1 \text{ mHz}$ [40, 44, 45, 46], is interrogated using a diode laser at 698 nm, which is prestabilized by locking it to a high-finesse ultrastable cavity, resulting in a laser optical linewidth below 1 Hz [47]. The probe beam is coaligned and copolarized with the optical lattice. To ensure that the stretched states are well resolved, the spectroscopy is performed under a magnetic bias field of $25 \mu\text{T}$, which results in a $\sim 250 \text{ Hz}$ separation between the two π -transitions excited during the spectroscopy.

Spectroscopy is performed using an 80-ms Rabi pulse, which when on resonance transfers a fraction of the atoms into the 3P_0 state. After applying the clock pulse, atoms remaining in the 1S_0 ground state are detected by measuring fluorescence on the strong $^1S_0 \rightarrow ^1P_1$ transition. The length of the pulse is long enough to measure both the population in the 1S_0 state as well as to heat these atoms out of the trap. The population in the 3P_0 state is then measured by first pumping the atoms back to the 1S_0 state through the intermediate $(5s5p)^3P_0 \rightarrow (5s6s)^3S_1$ and $(5s5p)^3P_2 \rightarrow (5s6s)^3S_1$ states and then by again measuring the fluorescence on the $^1S_0 \rightarrow ^1P_1$ transition. Combining these two measurements gives a normalized excitation fraction insensitive to atomic number fluctuations from shot to shot. A typical spectrum is shown in Fig. 1b. The Fourier-limited linewidth of the transition is 10 Hz, much less than the 250 Hz separation between the peaks, which makes the lines well resolved and also reduces potential line pulling effects due to any residual population left in other spin states by imperfect optical pumping. We note that while our optical local oscillator supports recovery of $< 2 \text{ Hz}$ spectroscopic linewidths [48], we find it more robust to run the clock transition with a 10 Hz Fourier-limited spectral linewidth.

To stabilize the optical local oscillator used for spectroscopy to the atomic transition, we use both stretched states. Using two time-multiplexed independent servos, we lock the laser frequency to the center of each transition. This is done by sampling the full width half maximum (FWHM)

of each transition (labeled $f_{1st\ lock}$ in Fig. 1b). The average of the two line centers gives the center frequency of the clock transition. The cavity-stabilized local oscillator, in combination with this frequency f_{center} , is in turn used to phase-lock a self-referenced octave-spanning optical frequency comb. The Sr-referenced repetition frequency of the comb is then counted with a H-maser located at NIST. A schematic of this locking setup is shown in Fig. 1c. Determination of the center frequency requires four experimental cycles, two for each of the $m_F = \pm 9/2$ transitions since a new atomic sample is reloaded for each lock point. The length of each experimental cycle is ≈ 1.1 s. After first probing the π transition for the $m_F = -9/2$ transition, we then probe the transition for the $m_F = +9/2$ state. The digital servo operates via standard modulation techniques. A linear feedback is also implemented to compensate for the drift of the high-finesse cavity used to prestabilize the clock laser. A second integration stage in the laser-atom feedback loop is used to calculate this feedback value (labeled $f_{2nd\ lock}$) in Fig. 1c. As shown in Fig. 1d, using this approach limits the residual drifts compensated for by the first servo integrator to typically < 1 mHz/s.

III. SYSTEMATIC SHIFTS OF THE STRONTIUM CLOCK

We have recently evaluated the systematic shifts of the strontium clock at the 1×10^{-16} level [1], and in Table I the important systematic shifts to the absolute frequency are shown. Although a detailed description can be found in [1], here we summarize these shifts. The evaluation of the systematic uncertainty is performed using the remotely located calcium optical standard at NIST [49], which is linked to JILA via a phase coherent optical fiber link [18]. The Sr-Ca comparison has a 1 s stability of 2×10^{-15} which averages down to below 3×10^{-16} after 200 s. To measure the Sr systematics an interleaved scheme is used where the Sr parameter of interest is varied between two different settings every 100 s, while the Ca standard remains locked. Pairs of such data are then used to determine the frequency shift, and many pairs are averaged in order to reach below the 10^{-16} level.

As shown in Table I, besides the correction that arises from the maser calibration, the dominant shift for the Sr clock is the black-body radiation (BBR)-induced shift. To determine this shift, the temperature of the Sr vacuum chamber is continuously monitored during the course of the absolute frequency measurement at four separate locations. During the measurement the average

Contributor	Correction (10^{-16})	Uncertainty (10^{-16})
Lattice Stark (scalar/tensor)	-6.5	0.5
Hyperpolarizability (lattice)	0.1	0.1
BBR Stark	54.0	1.0
AC Stark (probe beam)	0.15	0.1
1 st order Zeeman	0.2	0.2
2 nd order Zeeman	0.36	0.04
Density	3.8	0.5
Line pulling	0	0.2
Servo error	0	0.5
2 nd order Doppler	0	$\ll 0.01$
Sr Systematics Total	52.11	1.36
Maser calibration	-4393.7	8.5
Gravitational shift	12.5	1.0
Total	-4329.1	8.66
$\nu_{Sr} - \nu_0$	73.65 Hz	.37 Hz

TABLE I: Frequency corrections and their associated uncertainties for the clock transition in units of 10^{-16} fractional frequency, and with $\nu_0 = 429\,228\,004\,229\,800$ Hz. The maser correction uncertainty includes both Sr/H-Maser comparison, as well as the Cs clock uncertainty.

temperature of the chamber is 295(1) K, and the corresponding BBR effect:

$$\delta\nu_{BBR} = -2.354(32) \left(\frac{T}{300 \text{ K}} \right)^4 \text{ Hz} \quad (1)$$

gives a frequency shift of $54(1) \times 10^{-16}$. Higher-order multipoles are suppressed by α^2 and are negligible at this level. The given uncertainty in the BBR shift includes the error due to the chamber temperature, as well as the theoretical uncertainty in the polarizability [50].

For the duration of the experiment, the lattice laser is phase locked to the same optical frequency comb used to count the Sr beat, and the wavelength is simultaneously monitored on a wavemeter to ensure it does not mode-hop. The lattice is operated at a frequency of 368554.36(3) GHz [1, 8], slightly away from the state-insensitive lattice frequency. Including nuclear spin effects, the light shift due to the linearly polarized lattice can be expressed as [44]:

$$\delta\nu_S \approx -(\Delta\kappa^S - \Delta\kappa^T F(F+1)) \frac{U_T}{E_{rec}} - (\Delta\kappa^V m_F \xi \cos(\varphi) + \Delta\kappa^T 3m_F^2) \frac{U_T}{E_{rec}} \quad (2)$$

where $\Delta\kappa^{S,T,V}$ is the frequency shift coefficient due to the differential polarizability (scalar, tensor, and vector) between the ground and excited clock states, ξ is the degree of ellipticity of the beam (with $\xi = 0$ for π -polarized light), and φ is the angle between the lattice propagation direction

and the bias magnetic field ($\simeq \pi/2$ for our setup). For the linearly polarized lattice configuration in our setup, the vector light shift is minimized; furthermore since the Sr clock is operated using both the $m_F = \pm 9/2$ states, the antisymmetric m_F dependence averages away this vector shift. The effect of the tensor light shift for a given $|m_F|$ state introduces a polarization dependent offset to the state-insensitive lattice frequency. Experimentally, this Stark cancellation frequency for the $m_F = \pm 9/2$ state has been determined to be 368554.68(17) GHz [1] leading to a shift of $-6.5(5) \times 10^{-16}$ to the absolute clock frequency for the lattice depth and frequency used during this measurement. For our operating conditions, hyperpolarizability effects are more than an order of magnitude smaller [9, 41]. The ground and excited clock states have different polarizabilities at the clock transition frequency, and imperfect alignment between the clock laser and the lattice beam can lead to inhomogeneous Rabi frequencies in the transverse direction requiring an increase in the clock transition probe power. However, given the small saturation intensity of the clock probe beam, the ac Stark shift introduced by the clock laser during spectroscopy is small, and has been experimentally measured to be $0.15(10) \times 10^{-16}$. Stark shifts from laser beams not used during spectroscopy, for example those used for cooling and trapping during the MOT phase and for fluorescence detection after spectroscopy, are eliminated through the use of acousto-optic modulators (AOM) in series with mechanical shutters which block these beams during spectroscopy. In addition, the vacuum chamber is covered with an opaque cloth to prevent any stray light from entering the chamber.

For each experimental cycle sequence, the total atom number is recorded, allowing a point-for-point correction of the density shift. The value given in Table I is the average density correction. At the FWHM of the spectroscopic signal where the probe laser is locked, the excitation fraction in each stretched state is 15(2)%. This excitation fraction and our operating density of $\simeq 4 \times 10^{10} \text{cm}^{-3}$ gives a frequency correction of $3.8(5) \times 10^{-16}$ [1, 51].

The Zeeman shift of the transition frequency is given in Hz by [44]

$$\delta\nu_B \approx -\delta g m_F \mu_0 B + \beta B^2 \approx -1.084(4) \times 10^6 m_F B - 5.8(8) \times 10^{-8} B^2 \quad (3)$$

where $\mu_0 = \mu_B/h$, with μ_B the Bohr magneton, and δg the differential Landé g-factor between the ground and excited clock states. The 1st-order Zeeman shift is experimentally measured in [44], and the 2nd-order Zeeman shift is experimentally measured in [1], consistent with other measurements [52]. By measuring the average frequency of the stretched states at a small bias field, the 1st order Zeeman effect is averaged away due to the opposite linear dependence of the

shift on the $m_F = \pm 9/2$ states, and the experimentally measured value for the shift is consistent with zero. The bias field of $25 \mu\text{T}$ used during spectroscopy is large enough such that the spin states are well resolved, reducing line pulling effects due to residual populations in other states, yet small enough such that the 2^{nd} order Zeeman shift is negligible, with a value of $0.36(4) \times 10^{-17}$ for our bias field.

By operating in the Lamb-Dicke regime, 1^{st} order Doppler shifts are minimized. However, driven motion can also cause frequency shifts due to shaking of the lattice beams, or due to relative motion between the lattice and the probe beam. To minimize vibrations, the optics table is floated using standard pneumatic compressed air legs, and we estimate the effect of 1^{st} order Doppler shifts to be below 10^{-18} . Switching magnetic fields can also induce vibrations, however, our quadrupole trap is switched off more than 100 ms before spectroscopy. Furthermore, 2^{nd} -order Doppler effects from residual thermal motion are negligible ($< 10^{-18}$), given the $T = 2.5 \mu\text{K}$ temperature of the trapped Sr atoms.

The digital servos used to steer the spectroscopy laser to the atomic transition are another potential source of frequency offsets. The dominant cause of servo error is insufficient feedback gain to compensate for the linear drift of the high-finesse reference cavity. The second integration step as described in the experimental setup section reduces this effect. By analyzing our servo record we conservatively estimate this effect to be $< 5 \times 10^{-17}$. In conclusion, with the exception of the BBR-induced shift, all of the systematics discussed above are limited only by statistical uncertainty.

IV. FIBER TRANSFER BETWEEN JILA AND NIST

The strontium experiment is located at JILA, on the University of Colorado, Boulder campus and is linked to NIST Boulder Laboratories by a 3.5 km optical fiber network. To measure the absolute frequency of the transition, the tenth harmonic of the repetition rate of the frequency comb (which is phase-locked to the Sr clock laser and located at JILA), is beat against a ~ 950 MHz signal originating from NIST. A schematic of the transfer scheme from NIST is shown in Fig. 2. A 5 MHz signal from a hydrogen maser is distributed along a ~ 300 m cable to a distribution room where it is first frequency doubled and then used as a reference to stabilize an RF synthesizer operating near 950 MHz. In Fig. 2b, the stability of the H-maser as measured by Cs is shown, where the total length of the Sr absolute frequency measurement is indicated with a

dotted line. The RF signal generated by the synthesizer is then used to modulate the amplitude of a 1320 nm diode laser which is then transferred to JILA via the 3.5 km optical fiber link between the two labs [36, 37]. The microwave phase of the fiber link is actively stabilized using a fiber stretcher to control the group delay between NIST and JILA [37]. The limited dynamic range of the fiber stretcher necessitates a periodic change of the transfer frequency to relock the fiber transfer system for our 3.5 km link. Typically the dynamic range is sufficient to stabilize drifts for roughly 30-60 minute intervals, after which it must be unlocked and reset, leading to a dead time in the measurement of ~ 1 minute.

The transfer of the microwave signal between the NIST H-maser and JILA can potentially introduce a number of systematic frequency shifts and uncertainties. The majority of these arise from temperature-driven fluctuations during the course of the measurement. The microwave signal is transferred between the maser and the RF synthesizer using 300 m of cable after which it goes through a series of distribution amplifiers and a frequency doubler. All of the microwave electronics, as well as the cable used to transfer the signal, are sensitive to temperature-driven phase excursions. In order to correct for these effects, the temperature in the room is monitored continuously during the course of the experiment. In addition, the RF synthesizer is placed in a temperature-stabilized, thermally insulated box, and the temperature in the box is also continuously monitored. The temperature coefficient of the synthesizer is independently measured by applying a temperature ramp to the box while counting the frequency of the synthesizer relative to a second frequency stable synthesizer. The synthesizer is found to have a temperature coefficient of -3.6 ps/K, corresponding to a fractional frequency change of -1×10^{-15} for a temperature ramp of 1 K/h. This temperature coefficient is used to make rolling frequency corrections during the absolute frequency measurement.

To test the performance of the microwave electronics used for the modulation of the transfer laser as well as the fiber noise cancelation, an out-of-loop measurement is performed by detecting the heterodyne beat between the resulting transfer signal and the RF synthesizer. In Fig. 2c the Allan deviation is shown for this measurement, demonstrating that the fractional frequency instability due to these transfer components is 1×10^{-14} from 1-10 s, and averages down to $< 10^{-17}$ at 10^5 s. By correlating the out-of-loop measurement with temperature fluctuations in the distribution room during the course of the measurement, a temperature coefficient of $4.4 \times 10^{-16}/(\text{K/h})$ is found for the microwave electronics.

The distribution amplifiers, frequency doubler, and cable used to transfer the signal within the

distribution room are also tested by comparing the 10 MHz signal used to stabilize the synthesizer with a signal split off before the distribution amplifiers. This measurement determined a coefficient of $\sim 7 \times 10^{-16}/(\text{K/h})$.

The absolute frequency measurement, as discussed below in Section V, is recorded over 50 continuous hours. During the course of the absolute frequency measurement the insulated box used to house the RF synthesizer maintained an average temperature of 292.2(2) K, with a maximum slope of < 0.1 K/h. In Fig. 2d the black trace shows the resulting fractional frequency correction to the Sr frequency due to temperature-driven frequency fluctuations of the RF synthesizer. The total fractional correction to the Sr frequency due to the microwave electronics during the measurement, as well as the distribution amplifiers and cables, is shown by the grey trace in Fig. 2d. During hour 37 (133×10^3 s) of the measurement, a temperature ramp began in the distribution room, leading to a large slope in the temperature during hour 37 and during hour 50 (180×10^3 s) as the temperature restabilized. However, this transient affected only a small fraction of the data. Using the measured temperature coefficients, a rolling correction is made to all of the measured frequencies. The average frequency correction during the course of the measurement is 9×10^{-17} , with an uncertainty of 1×10^{-17} . These corrections do not influence the statistics of the final absolute frequency measurement. In other words, the final mean frequency and standard error are the same with and without these corrections.

V. FREQUENCY MEASUREMENT RESULTS

As shown in Fig. 2b, the Allan deviation of the H-maser averages down as $\sim 3 \times 10^{-13}/\sqrt{\tau}$. To measure the Sr absolute frequency to below 10^{-15} , the measurement is performed for 50 continuous hours. The largest frequency correction to the measured ^{87}Sr frequency is the calibration offset of the H-maser frequency. The H-maser is simultaneously counted against the Cs standard during the duration of the measurement and the resulting frequency correction to the $^{87}\text{Sr}/\text{H}$ -maser comparison is $-439.37(85) \times 10^{-15}$, where the uncertainty includes both an uncertainty of 0.6×10^{-15} due to the Cs standard, as well as an uncertainty of 0.6×10^{-15} from dead time in the Sr/H-maser measurement. An additional frequency correction is the gravitational shift due to the difference in elevation between the Cs laboratory at NIST and the Sr laboratory at JILA. The difference in elevation between the two labs, which has been determined using GPS receivers located in each building to be 11.3(2) m, gives a frequency shift of $12.5(1.0) \times 10^{-16}$, where the given uncertainty

includes the uncertainty in the elevation as well as the uncertainty due to the geoid correction [53].

In Fig. 3, the 50 hour counting record is shown for the Sr frequency, with a 30 s gate time. The frequency shown includes only the correction due to the maser, and is plotted with an offset frequency of $\nu_0 = 429\,228\,004\,229\,800$ Hz. The frequency excursions and gaps seen in Fig. 3a occur when the Sr system is unlocked, which happens when either the frequency comb comes unlocked, or when the probe laser is not locked to the atomic signal. During the course of the measurement the lattice intensity and frequency, all laser locks, and the temperature at both JILA and in the distribution room in NIST are continuously monitored and recorded. In Fig. 3b, data corresponding to times when any lasers are unlocked, including times when the spectroscopy laser is not locked to the atoms, and times when the lattice laser intensity or frequency is incorrect, have been removed. In Fig. 4a, a histogram of this final counting record is shown, demonstrating the gaussian statistics of the measurement. The mean value (relative to ν_0) of the measured frequency is 70.88(35) Hz. In Fig. 4b the Total deviation of the frequency measurement is shown. The Total deviation [54] is similar to the Allan deviation, however it is better at predicting the long-term fractional frequency instability. The 1-s stability of the H-maser used for the measurement is 1.5×10^{-13} . However, from a fit to the Total deviation, we find a 1-s stability of $\sigma_{1s} = 2.64(8) \times 10^{-13}$ for the counting record, which is limited by counter noise, and averages down as $\sigma_{1s} / \tau^{0.48(1)}$. Extrapolating to the full length of the data set (excluding dead time in the measurement) gives a statistical uncertainty of 8×10^{-16} . The frequency uncertainty of Sr is low enough such that this uncertainty is dominated by the performance of the maser (see Fig. 4b), which is included in the maser calibration uncertainty given in Table I.

Including the uncertainty of the H-maser as well as the strontium systematics described in Section III gives a final frequency of 429 228 004 229 873.65 (37) Hz, where the dominant uncertainty is due to the H-maser calibration. In Fig. 5, this measurement is compared with previous Sr frequency measurements by this group [8, 33, 55, 56], as well as by the Paris [9, 35] and Tokyo [34] groups. As shown in the figure, the agreement between international measurements of the Sr frequency is excellent, with the most recent measurements in agreement below the 10^{-15} level, making the Sr clock transition the best agreed upon optical frequency standard to date. The high level of agreement enabled a recent analysis of this combined data set that constrains the coupling of fundamental constants to the gravitational potential as well as their drifts [22].

VI. CONCLUSION

In conclusion, we have made an accurate measurement of the $^1S_0-^3P_0$ clock transition in fermionic strontium, where the final fractional uncertainty of 8.6×10^{-16} is limited primarily by the performance of the intermediate hydrogen maser used to compare the Sr standard to the NIST-F1 Cs fountain clock. This experiment represents one of the most accurate measurements of an optical frequency to date, and the excellent agreement with previous measurements makes strontium an excellent candidate for a possible redefinition of the SI second in the future. In addition, the combined frequency measurements of ^{87}Sr performed worldwide, as well as future measurements of frequency ratios with other optical standards can be used to search for time-dependent frequency changes which constrain variations of fundamental constants [22].

VII. ACKNOWLEDGEMENT

We gratefully thank S. Foreman and D. Hudson for their contribution to the noise-cancelled fiber network, T. Fortier, J. Stalnaker, Z. W. Barber, and C. W. Oates for the Sr - Ca optical comparison, and J. Levine for help with the Cs-Sr elevation difference. We acknowledge funding support from NIST, NSF, ONR, and DARPA. G. Campbell is supported by a National Research Council postdoctoral fellowship, M. Miranda is supported by a CAPES/Fullbright scholarship, and J. W. Thomsen is a JILA visiting fellow, his permanent address is The Niels Bohr Institute, Universitetsparken 5, 2100 Copenhagen, Denmark.

-
- [1] A. D. Ludlow, T. Zelevinsky, G. K. Campbell, S. Blatt, M. M. Boyd, M. H. G. de Miranda, M. J. Martin, J. W. Thomsen, S. M. Foreman, J. Ye, et al., *Science* **319**, 1805 (2008).
 - [2] T. Rosenband, D. B. Hume, P. O. Schmidt, C. W. Chou, A. Brusch, L. Lorini, W. H. Oskay, R. E. Drullinger, T. M. Fortier, J. E. Stalnaker, et al., *Science* **319**, 1808 (2008).
 - [3] W. H. Oskay, S. A. Diddams, E. A. Donley, T. M. Fortier, T. P. Heavner, L. Hollberg, W. M. Itano, S. R. Jefferts, M. J. Delaney, K. Kim, et al., *Phys. Rev. Lett.* **97**, 020801 (2006).
 - [4] H. S. Margolis, G. P. Barwood, G. Huang, H. A. Klein, S. N. Lea, K. Szymaniec, and P. Gill, *Science* **306**, 1355 (2004).

- [5] P. Dubé, A. A. Madej, J. E. Bernard, L. Marmet, J.-S. Boulanger, and S. Cundy, *Phys. Rev. Lett.* **95**, 033001 (2005).
- [6] T. Schneider, E. Peik, and C. Tamm, *Phys. Rev. Lett.* **94**, 230801 (2005).
- [7] M. Takamoto, F. Hong, R. Higashi, and H. Katori, *Nature* **435**, 321 (2005).
- [8] A. D. Ludlow, M. M. Boyd, T. Zelevinsky, S. M. Foreman, S. Blatt, M. Notcutt, T. Ido, and J. Ye, *Phys. Rev. Lett.* **96**, 033003 (2006).
- [9] R. L. Targat, X. Baillard, M. Fouché, A. Bruschi, O. Tcherbakoff, G. D. Rovera, and P. Lemonde, *Phys. Rev. Lett.* **97**, 130801 (2006).
- [10] Z. W. Barber, J. E. Stalnaker, N. D. Lemke, N. Poli, C. W. Oates, T. M. Fortier, S. A. Diddams, L. Hollberg, C. W. Hoyt, A. V. Taichenachev, et al., *Physical Review Letters* **100**, 103002 (2008).
- [11] U. Sterr, C. Degenhardt, H. Stoeckl, C. Lisdat, H. Schnatz, J. Helmcke, F. Riehle, G. Wilpers, C. Oates, and L. Hollberg, *Comptes Rendus Physique* **5**, 845 (2004).
- [12] J. Keupp, A. Douillet, T. E. Mehlstäubler, N. Rehbein, E. M. Rasel, and W. Ertmer, *Eur. Phys. J. D* **36**, 289 (2005).
- [13] G. Wilpers, C. Oates, and L. Hollberg, *Applied Physics B: Lasers and Optics* **85**, 31 (2006).
- [14] T. P. Heavner, S. R. Jefferts, E. A. Donley, J. H. Shirley, and T. E. Parker, *Metrologia* **42**, 411 (2005).
- [15] S. Bize, P. Laurent, M. Abgrall, H. Marion, I. Maksimovic, L. Cacciapuoti, J. Grünert, C. Vian, F. P. D. Santos, P. Rosenbusch, et al., *Journal of Physics B: Atomic, Molecular and Optical Physics* **38**, S449 (2005).
- [16] S. Weyers, U. Hübner, R. Schröder, C. Tamm, and A. Bauch, *Metrologia* **38**, 343 (2001).
- [17] T. E. Parker, *Proceedings of the 22nd European Frequency and Time Forum* p. to be published (2008).
- [18] S. M. Foreman, A. D. Ludlow, M. H. G. de Miranda, J. E. Stalnaker, S. A. Diddams, and J. Ye, *Phys. Rev. Lett.* **99**, 153601 (2007).
- [19] F. Narbonne, M. Lours, S. Bize, A. Clairon, G. Santarelli, O. Lopez, C. Daussy, A. Amy-Klein, and C. Chardonnet, *Rev. Sci. Instrum.* **77**, 064701 (2006).
- [20] I. Coddington, W. C. Swann, L. Lorini, J. C. Bergquist, Y. L. Coq, C. W. Oates, Q. Quraishi, K. S. Feder, J. W. Nicholson, P. S. Westbrook, et al., *Nat. Photon.* **1**, 283 (2007).
- [21] O. Lopez, A. Amy-Klein, C. Daussy, C. Chardonnet, F. Narbonne, M. Lours, and G. Santarelli, *Arxiv preprint arXiv:0711.0933* (2007).
- [22] S. Blatt, A. D. Ludlow, G. K. Campbell, J. Thomsen, T. Zelevinsky, M. M. Boyd, J. Ye, X. Baillard, M. Fouché, R. L. Targat, et al., *Phys. Rev. Lett.* **100**, 140801 (2008).

- [23] H. Marion, F. Pereira Dos Santos, M. Abgrall, S. Zhang, Y. Sortais, S. Bize, I. Maksimovic, D. Calonico, J. Grünert, C. Mandache, et al., *Phys. Rev. Lett.* **90**, 150801 (2003).
- [24] M. Fischer, N. Kolachevsky, M. Zimmermann, R. Holzwarth, T. Udem, T. W. Hänsch, M. Abgrall, J. Grünert, I. Maksimovic, S. Bize, et al., *Phys. Rev. Lett.* **92**, 230802 (2004).
- [25] E. Peik, B. Lipphardt, H. Schnatz, T. Schneider, C. Tamm, and S. G. Karshenboim, *Phys. Rev. Lett.* **93**, 170801 (2004).
- [26] S. Bize, P. Laurent, M. Abgrall, H. Marion, I. Maksimovic, L. Cacciapuoti, J. Grünert, C. Vian, F. P. D. Santos, P. Rosenbusch, et al., *J. Phys. B* **38**, S449 (2005).
- [27] E. Peik, B. Lipphardt, H. Schnatz, C. Tamm, S. Weyers, and R. Wynands, *Arxiv preprint physics/0611088* (2006).
- [28] S. N. Lea, *Rep. Prog. Phys.* **70**, 1473 (2007).
- [29] T. M. Fortier, N. Ashby, J. C. Bergquist, M. J. Delaney, S. A. Diddams, T. P. Heavner, L. Hollberg, W. M. Itano, S. R. Jefferts, K. Kim, et al., *Phys. Rev. Lett.* **98**, 070801 (2007).
- [30] V. M. Flambaum and A. F. Tedesco, *Phys. Rev. C* **73**, 055501 (2006).
- [31] N. Ashby, T. P. Heavner, S. R. Jefferts, T. E. Parker, A. G. Radnaev, and Y. O. Dudin, *Phys. Rev. Lett.* **98**, 070802 (2007).
- [32] A. Bauch and S. Weyers, *Phys. Rev. D* **65**, 081101 (2002).
- [33] M. M. Boyd, A. D. Ludlow, S. Blatt, S. M. Foreman, T. Ido, T. Zelevinsky, and J. Ye, *Phys. Rev. Lett.* **98**, 083002 (2007).
- [34] M. Takamoto, F. Hong, R. Higashi, Y. Fujii, M. Imae, and H. Katori, *J Phys. Soc. Jpn.* **75**, 104302 (2006).
- [35] X. Baillard, M. Fouché, R. L. Targat, P. G. Westergaard, A. Lecallier, F. Chapelet, M. Abgrall, G. D. Rovera, P. Laurent, P. Rosenbusch, et al., published online in *Eur. Phys. J. D* (2008).
- [36] J. Ye, J.-L. Peng, R. J. Jones, K. W. Holman, J. L. Hall, D. J. Jones, S. A. Diddams, J. Kitching, S. Bize, J. C. Bergquist, et al., *J. Opt. Soc. Am. B* **20**, 1459 (2003).
- [37] S. M. Foreman, K. W. Holman, D. D. Hudson, D. J. Jones, and J. Ye, *Rev. Sci. Inst.* **78**, 021101 (2007).
- [38] T. Mukaiyama, H. Katori, T. Ido, Y. Li, and M. Kuwata-Gonokami, *Phys. Rev. Lett.* **90**, 113002 (2003).
- [39] T. H. Loftus, T. Ido, A. D. Ludlow, M. M. Boyd, and J. Ye, *Phys. Rev. Lett.* **93**, 073003 (2004).
- [40] H. Katori, M. Takamoto, V. G. Pal'chikov, and V. D. Ovsiannikov, *Phys. Rev. Lett.* **91**, 173005 (2003).
- [41] A. Bruschi, R. L. Targat, X. Baillard, M. Fouché, and P. Lemonde, *Phys. Rev. Lett.* **96**, 103003 (2006).

- [42] D. Leibfried, R. Blatt, C. Monroe, and D. Wineland, *Rev. Mod. Phys.* **75**, 281 (2003).
- [43] P. Lemonde and P. Wolf, *Phys. Rev. A* **72**, 033409 (2005).
- [44] M. M. Boyd, T. Zelevinsky, A. D. Ludlow, S. Blatt, T. Zanon-Willette, S. M. Foreman, and J. Ye, *Phys. Rev. A* **76**, 022510 (2007).
- [45] R. Santra, K. V. Christ, and C. H. Greene, *Phys. Rev. A* **69**, 042510 (2004).
- [46] S. G. Porsev and A. Derevianko, *Phys. Rev. A* **69**, 042506 (2004).
- [47] A. D. Ludlow, X. Huang, M. Notcutt, T. Zanon-Willette, S. M. Foreman, M. M. Boyd, S. Blatt, and J. Ye, *Opt. Lett.* **32**, 641 (2007).
- [48] M. M. Boyd, T. Zelevinsky, A. D. Ludlow, S. M. Foreman, S. Blatt, T. Ido, and J. Ye, *Science* **314**, 1430 (2006).
- [49] C. Oates, C. Hoyt, Y. Coq, Z. Barber, T. Fortier, J. Stalnaker, S. Diddams, and L. Hollberg, *International Frequency Control Symposium and Exposition, 2006 IEEE* p. 74 (2006).
- [50] S. G. Porsev and A. Derevianko, *Phys. Rev. A* **74**, 020502 (2006).
- [51] A. D. Ludlow and et al., to be published (2008).
- [52] X. Baillard, M. Fouché, R. L. Targat, P. G. Westergaard, A. Lecallier, Y. L. Coq, G. D. Rovera, S. Bize, and P. Lemonde, *Opt. Lett.* **32**, 1812 (2007).
- [53] The geoid correction was determined using National Geodetic Survey benchmarks located on both the University of Colorado campus and the NIST campus, which have all been corrected using the GEOID03 model. Using these benchmarks, the geoid height between NIST and JILA varies by less than 0.10 m.
- [54] C. Greenhall, D. Howe, and D. Percival, *IEEE Trans.Ultrason. Ferroelectr. Freq. Control* **46**, 1183 (1999).
- [55] M. M. Boyd, A. D. Ludlow, T. Zelevinsky, S. M. Foreman, S. Blatt, T. Ido, and J. Ye, in *Proceedings of the 20th European Frequency and Time Forum* (2006), p. 314.
- [56] J. Ye, S. Blatt, M. M. Boyd, S. M. Foreman, E. R. Hudson, T. Ido, B. Lev, A. D. Ludlow, B. C. Sawyer, B. Stuhl, et al., in *Atomic Physics 20*, edited by C. Roos, H. Häffner, and R. Blatt (2006).

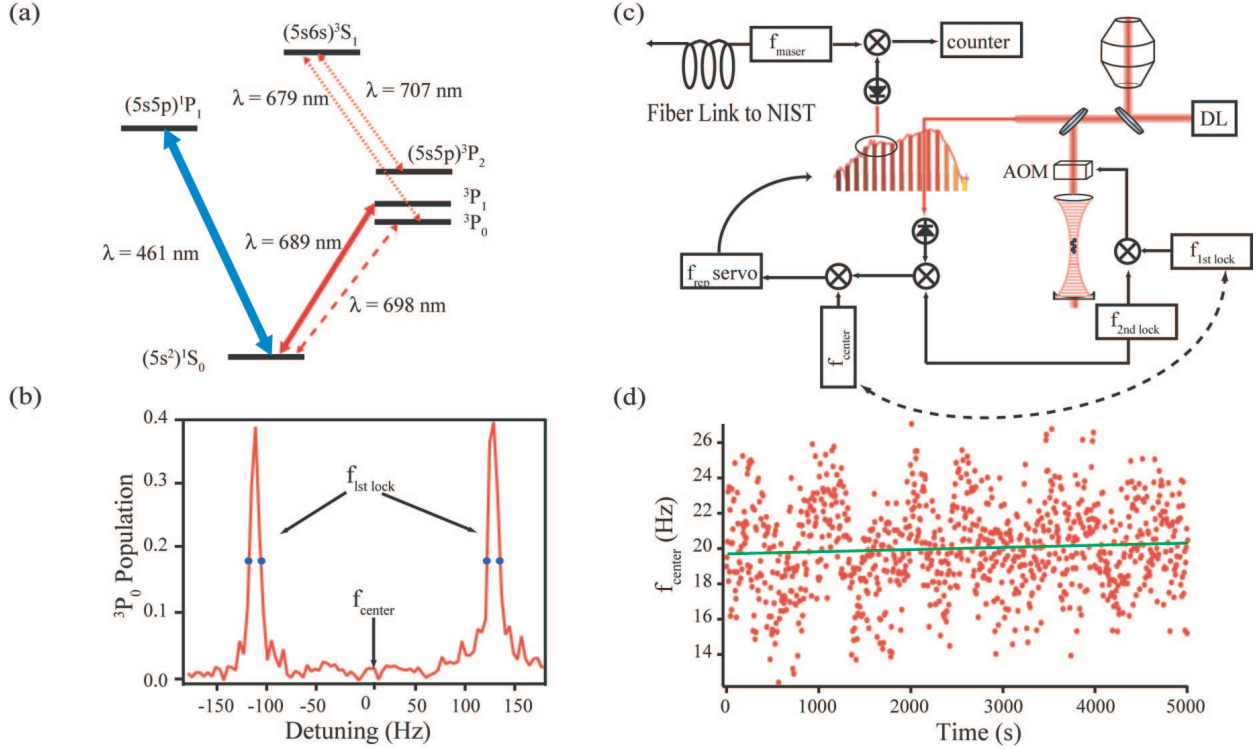


FIG. 1: Experimental Setup. (a) Relevant energy levels for ^{87}Sr used for the optical lattice clock. Transitions at 461 nm and 689 nm are used in two-stage cooling and trapping of the Sr atoms. The clock transition is at 698 nm. Lasers at 679 and 707 nm provide necessary repumping from metastable states. (b) To operate the clock, ultracold ^{87}Sr atoms are first optically pumped to the $|F = 9/2, m_f = \pm 9/2\rangle$ states. The clock center frequency (f_{center}) is found by locking the probe laser frequency to both peaks successively and taking their average. The laser is locked to the center of each transition by sampling their FWHM as illustrated in the figure by dots ($f_{1st\ lock}$). (c) Schematic of the setup used for locking the optical local oscillator to the ^{87}Sr transition. The clock transition is probed using a diode laser (DL) at $\lambda = 698$ nm which is locked to an ultrastable, high finesse optical cavity. The laser beam is used to interrogate the Sr atoms and is transferred to the atoms using an optical fiber with active fiber noise cancellation. To steer the frequency of the laser for the lock to the Sr resonance, an acousto-optic modulator (AOM) is used to introduce a frequency offset between the cavity and the atoms. The frequency offset is steered to the lock points ($f_{1st\ lock}$). The frequency offset also includes a linear feedback value ($f_{2nd\ lock}$) to compensate for the linear drift of the high finesse cavity. The cavity-stabilized clock laser is also used to phase-lock a self-referenced octave-spanning optical frequency comb, in combination with atomic resonance information contained in f_{center} and $f_{2nd\ lock}$. The Sr-referenced repetition frequency of the comb (f_{rep}) is then counted relative to a H-maser located at NIST (f_{maser}). (d) Sample data showing the in-loop atom lock for 5000 s of data taken during the measurement of the absolute frequency. The fit gives a residual linear fractional frequency drift of $< 2 \times 10^{-19}/\text{s}$.

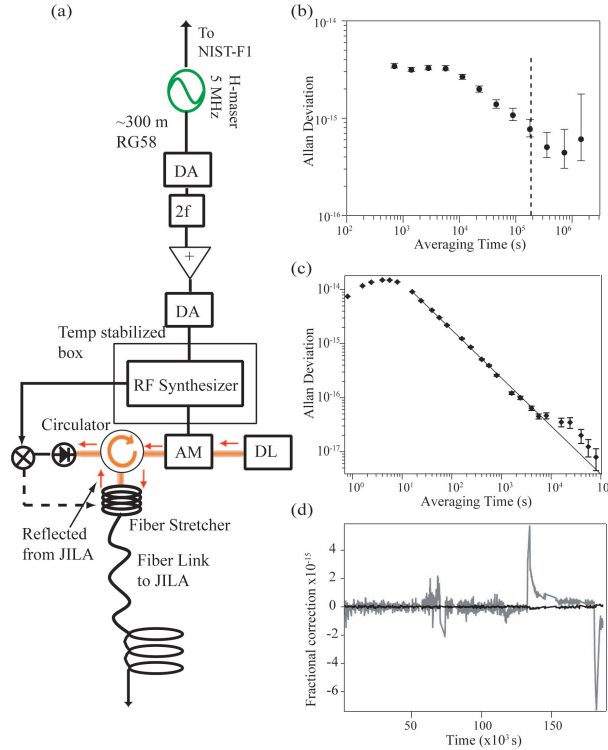


FIG. 2: Clock signal transfer between NIST and JILA. (a) Schematic of the setup used to transfer the hydrogen maser signal from NIST to JILA. A 5 MHz signal from the H-maser, which is simultaneously counted against the NIST-F1 Cs standard, is distributed through a ~ 300 m cable to a distribution amplifier (DA). After the distribution amplifier it is actively frequency doubled ($2f$) and sent through a second distribution amplifier. The resulting 10 MHz signal is used to reference an RF Synthesizer operating at ~ 950 MHz. The synthesizer in turn modulates the amplitude (AM) of a 1320 nm laser (DL) which is transferred to JILA through a 3.5 km fiber link. Noise from the fiber link is canceled with a fiber stretcher to actively stabilize the microwave phase using a retroreflection of the beam sent back from JILA [37]. (b) Typical Allan deviation of the H-maser used for the Sr absolute frequency measurement, with the total duration of the measurement represented by a dotted line. (c) Out of loop measurement of the stability of the microwave electronics used for transfer and fiber noise cancelation. The fit to the line gives a 1-s Allan deviation of $1.08(1) \times 10^{-13}$ with a slope of $-0.889(4)$. The bump at 10000 s is indicative of temperature fluctuations in the distribution room during the out of loop measurement. The bump at 10 s is due to low pass filtering of the phase measurement. (d) Frequency correction due to temperature fluctuations in the distribution room (grey curve) and fluctuations in the temperature-stabilized box used to house the RF synthesizer (black curve) during the course of the measurement.

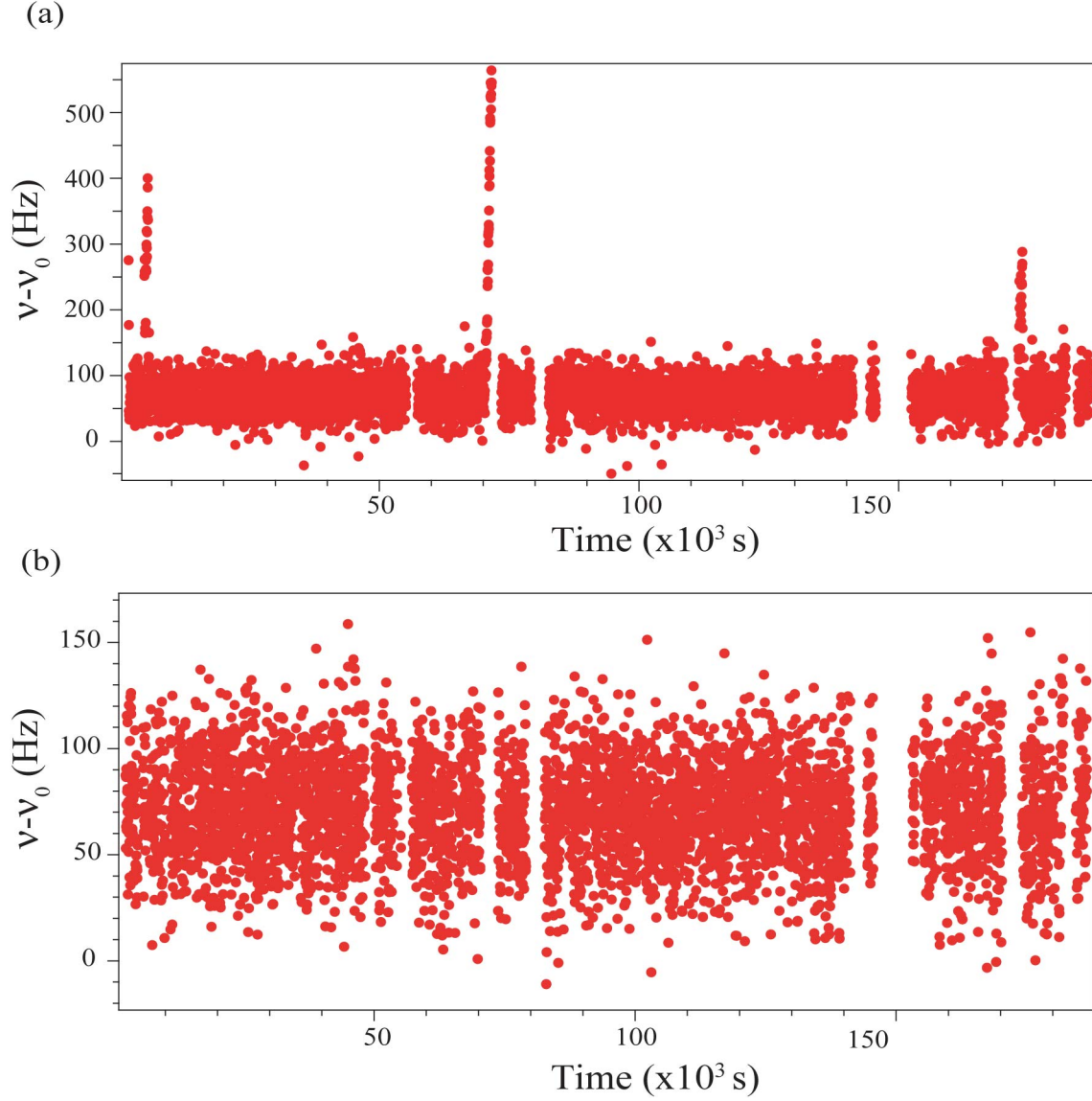


FIG. 3: Absolute frequency measurements of the $^1S_0-^3P_0$ clock transition. (a) Counting record showing all of the data taken over a 50 hour period. Each point corresponds to a 30 s average, and the overall offset is $\nu_0 = 429\,228\,004\,229\,800$ Hz. (b) The counting record after removing points where the system is not locked. The mean value is $70.88(35)$ Hz.

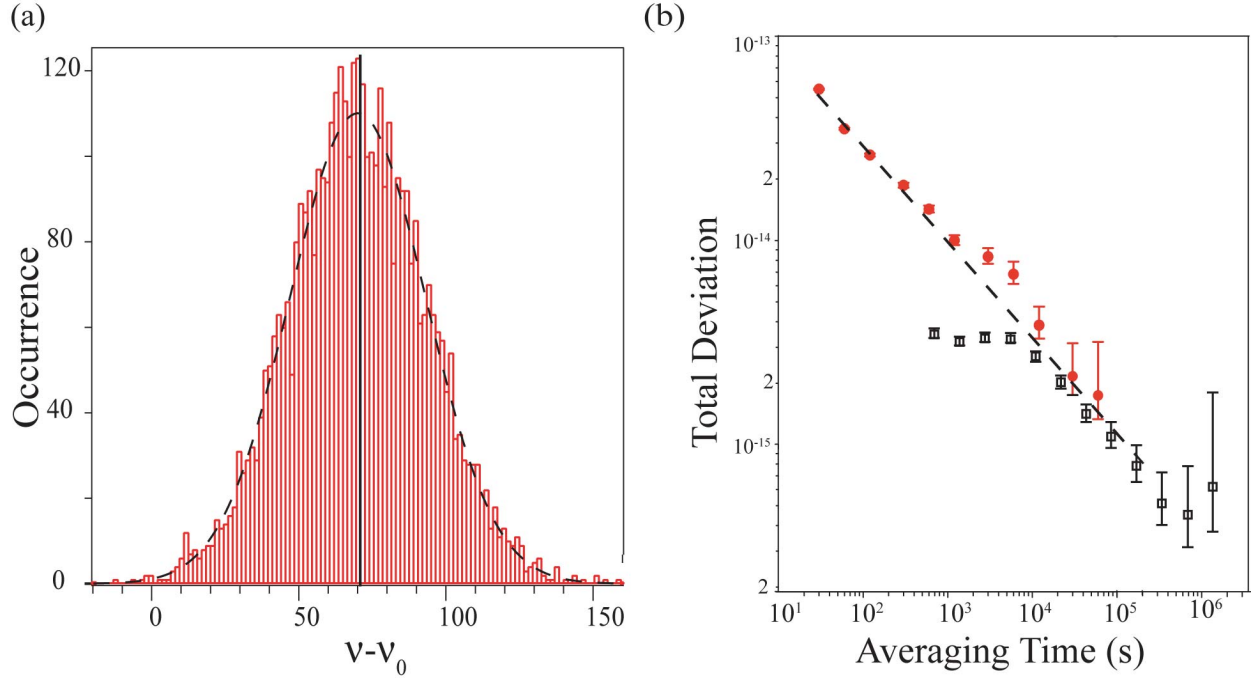


FIG. 4: (a) Histogram of the frequency measurements shown in Fig. 3, including the maser correction. The dashed line is a gaussian fit to the data, the mean frequency is 70.88 Hz and is indicated by the black line. (b) Total Deviation of the frequency measurement for the Sr/H-maser comparison (circles), and the H-maser/Cs comparison (squares). The dotted line shows a fit of the Sr deviation to $a\tau^{-b}$, where $a = 2.64(8) \times 10^{-13}$ and $b = 0.48(1)$, and the dotted line extends out to the full measurement time. For averaging times $\tau > 10^4$ s, the maser noise dominates both the Cs/H-maser and the Sr/H-maser measurement, and hence the maser uncertainty (6×10^{-16} , as described in the text) needs to be counted only once in the final Sr/Cs measurement uncertainty budget.

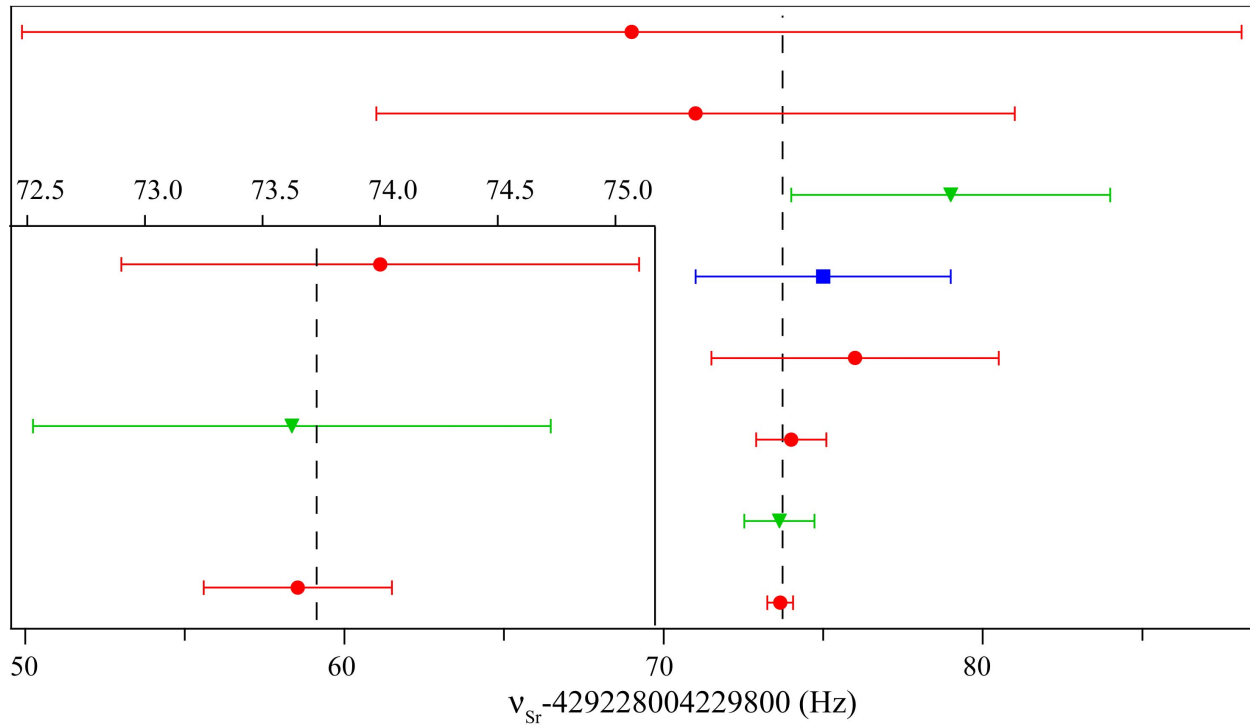


FIG. 5: Record of Sr absolute frequency measurements. Previous measurements by this group (circles) [8, 33, 55, 56], as well as the Paris (triangle) [9, 35] and Tokyo (square) [34] groups are shown. The inset shows the high agreement of the most recent measurements which agree below the 10^{-15} level. The dashed line shows the weighted mean, $\bar{\nu} = 429\,228\,004\,229\,873.73$ Hz of the combined data set.